Available online at www.sciencedirect.com
ScienceDirect
Journal of the European Ceramic Society 28 (2008) 1801–1808
www.elsevier.com/locate/jeurceramsoc

Processing of YSZ screen printing pastes and the characterization of the electrolyte layers for anode supported SOFC

Peter Ried [a,*], Christiane Lorenz [a], Anke Brönstrup [a], Thomas Graule [a], Norbert H. Menzler [c], Werner Sitte [b], Peter Holtappels [a]

[a] *Empa, Swiss Federal Laboratories for Materials Testing and Research, Laboratory for High Performance Ceramics, Überlandstrasse 129, CH-8600 Dübendorf, Switzerland*
[b] *Chair of Physical Chemistry, University of Leoben, Franz-Josef-Strasse 18, A-8700 Leoben, Austria*
[c] *Forschungszentrum Jülich, Institute of Energy Research, IEF-1, 52425 Jülich, Germany*

Received 22 July 2007; received in revised form 12 November 2007; accepted 16 November 2007
Available online 14 February 2008

Abstract

Screen printing pastes based on organic binder systems were developed for the production of dense electrolyte layers of $Y_{0.16}Zr_{0.84}O_{1.92}$(8YSZ) on Ni/YSZ anode substrates for anode supported solid oxide fuel cells (SOFCs). Pastes with a solid loading up to 50 vol.% (86 wt.%) of YSZ powder and the adequate thixotropic behaviour for screen printing could be produced. Dense layers were obtained by sintering at 1430 °C and were shown to be gas tight by window and He leakage test. The electrical conductivity of the dense layers and the resulting activation energy (96–99 kJ mol^{-1}) were obtained from impedance spectra in the temperature range from 250 °C to 900 °C. The agreement with literature values indicates that performing layers have been obtained.

Keywords: Screen printing; Electron microscopy; Impedance; ZrO_2; Fuel cells

1. Introduction

Solid oxide fuel cells based on ceramic materials are promising devices converting hydrocarbon fuels to electrical energy with high efficiency.[1] Both cathode and anode materials are electronic conductors with catalytic activity, while the gas tight electrolyte of around 20 μm thickness in between is an ionic conductor. Screen printing is an industrially used cost-effective method to fabricate homogeneous layers of pastes containing ceramic powders. Organic binder systems are frequently used for large-scale production such as lacquers[2] because they are insensitive to seasonal changes of temperature and humidity compared to water-based dispersions. Zirconia dispersions with a high solid loading have already been presented previously. Zuercher et al.[3] showed the possibility to produce low-viscosity suspensions and identified Solsperse 3000 as a dispersant and terpineol among other organic media as most suitable for dispersions of YSZ powder.

Sintering of dense electrolyte layers usually requires temperatures above 1400 °C. However, these high temperatures pose severe problems on the co-firing of all cell components. This might cause coarsening of the microstructure of the Ni–YSZ cermet and can lead to interfacial reactions between the cathode materials and the electrolyte material[4] forming, e.g. $La_2Zr_2O_7$. The grain coarsening leads to a reduced active area for the catalytic reactions on the anode and the interfacial reactions to less active areas on the cathode side.

The development of organic-based slurries to achieve gas tight electrolyte layers at standard sintering conditions was the main goal of this study. The study of the sintering behaviour at lower temperatures could give information about further necessary modifications in the paste recipe. A reduction of the sintering temperature while still achieving gas tight electrolyte layers is expected to result in more durable, high performing electrode microstructures and reduced production costs.

* Corresponding author. Tel.: +41 44 823 41 72.
E-mail address: peter.ried@empa.ch (P. Ried).

0955-2219/$ – see front matter © 2008 Elsevier Ltd. All rights reserved.
doi:10.1016/j.jeurceramsoc.2007.11.018

Table 1
Raw materials used for the preparation of YSZ screen printing pastes

Provider	Denotation	Density/BET/d_{50}	Chem. nature	Usage
Unitec	FYT13-002H	–/4.31 m^2/g/0.56 μm	$Y_{0.16}Zr_{0.84}O_{1.92}$	Electrolyte
Tosoh	TZ8-YS	–/6.01 m^2/g/0.37 μm	$Y_{0.16}Zr_{0.84}O_{1.92}$	Electrolyte
Fluka	Terpinol	$\rho = 0.93$ g/cm^3/–	Terpene	Solvent
Avecia Additives	Solsperse 3000	$\rho = 0.91$ g/cm^3/–	Organic oligomer	Dispersant
Fluka	PVP[a]	–	Organic polymer	Dispersant
Clariant	PVB[b] (B30H)	$\rho = 1.1$ g/cm^3/–	Organic polymer	Binder
	PVB[b] (B20H)	$\rho = 1.1$ g/cm^3/–	Organic polymer	Binder

[a] Polyvinylpyrrolidon.
[b] Polyvinylbutyral.

2. Experimental

The pastes, produced for this study, contained terpineol as a solvent, one of two different zirconia powders (both 8 mol% yttria stabilized zirconia), Solsperse 3000 a commercially available penta-(12-hydroxystearic acid) or polyvinylpyrrolidon as dispersant and polyvinylbutyral as a binder. Table 1 summarizes the material properties and suppliers.

The solid loading of the electrolyte powder was calculated in vol.% of the final paste, the amount of dispersant depending on the specific surface area of the powder and the binder in wt.% of the powder. After mixing the dispersant and the binder with the solvent the YSZ powder was added in small portions while stirring the slurry with an automatic stirrer and subsequently the paste was homogenized with a 3-roll mill (EXAKT-Dreiwalzenwerk).

The rheological behaviour of the pastes was tested with a rotational viscosimeter (Rheolab MC120, Physica Messtechnik GmbH, Germany) with a volume of 3 cm^3 and a gap of 0.59 mm between the two cylinders at 25 °C. The viscosity of the pastes was measured for shear rates between 1 s^{-1} and 300 s^{-1} repeating 3 times to ensure good reproducibility.

The anode substrates (50 vol.% NiO/YSZ) were pressed with an automatic uniaxial press (Römheld, Germany) at a pressure of 100 MPa using a laboratory made nickel/YSZ spray dried cermet powder granulate. The anode substrates were partly pre-sintered at 1200 °C to reduce the bending of the samples during co-sintering with the electrolyte layers. The open porosity of the cermet granules was preserved and the binder is entirely removed at this temperature.

Two different screens and scrapers for printing were used. Out of the four combinations of a fine screen or a coarse screen (325 mesh or 255 mesh, respectively) combined with a soft scraper with round edges, or a stiff scraper and sharp edges, the stiff scraper with the coarser screen was the best system to print homogeneous layers with the applicable slurries. After printing the slurries on the anode substrates (with and without pre-sintering) the samples were dried overnight and co-sintered with the temperature profile shown in Table 2.

Additionally, anode substrates were prepared from coarse and fine Ni–YSZ granulates: YSZ layers were printed on pre-sintered and on green anode substrates and co-sintered at temperatures between 1250 °C and 1430 °C for 2 h or 12 h.

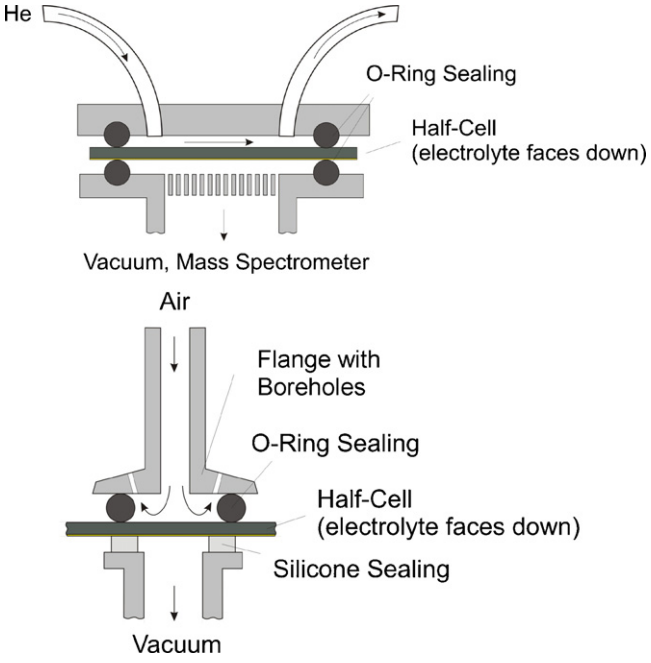

Fig. 1. Top: principle setup for the He leak test, bottom: setup for the window leak test[6].

The sintered electrolyte layers were examined after sintering by SEM (Tescan TS51368M), the gas tightness was checked by both He leakage test and window leak test[5,6] as shown in Fig. 1. The samples are put into a sample holder with the electrolyte side facing the vacuum.

Principally, the window leak test measures effectively the permeation, in this case of air through the sample depending on the pressure difference between the surrounding area and the drawn vacuum. After reaching a constant vacuum ($\Delta p = 100$ mbar) the chamber is closed and the time dependent increase of pressure within the chamber is recorded. The permeability coefficient (k)

Table 2
Co-sintering programme

Segment	1	2	3	4	5	6
Ramp (°C/h)	60	600	300	60	60	300
Level max (°C)	300	800	1100	T_{max}	$T_{max} - 80$	25
Holding time (h)	None	None	None	2 or 12	None	End

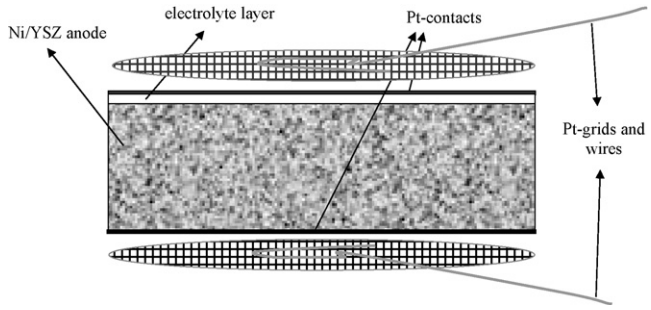

Fig. 2. Sample with contacts for the impedance measurement in a reducing atmosphere.

is calculated directly from the pressure according to the following equation (calculation of the permeability coefficient from window leak test):

$$k(L)\,[\mathrm{cm}^2/\mathrm{s}] = \frac{\Delta p_i}{\Delta t} \cdot V \cdot \frac{l}{A} \cdot \frac{1}{\Delta \bar{p}}$$

The internal pressure difference (Δp_i) inside the vacuum chamber during a time interval (Δt) is related to the mean pressure difference $\Delta \bar{p}$ between the outside and the vacuum chamber and normalized to the gas volume (V) on the vacuum side, the diffusion length (l) and the sample area (A).

The principal of the helium leakage test is similar, except the substrate side is floated with gaseous helium and the permeating He is measured with a mass spectrometer and converted into the permeation rate (hPa dm^3/s). This value has to be divided by the sample's area and a factor of 10 (considering on one hand side the pressure difference of about 100 hPa between cathode and anode during operation of the fuel cell and on the other hand the pressure difference at which the leak rate is determined which is approximately 1000 hPa).

The conductivity of the YSZ layers of selected gas tight samples was measured by impedance spectroscopy. The samples were painted on both the YSZ electrolyte layer and the Ni-cermet with Pt-paste and contacted by Pt-grids as shown in Fig. 2.

Table 3
Anode substrates before and after pre-sintering

	Height (mm) (±0.05)	Diameter (mm) (±0.01)	Weight (g) (±0.1)
Green	0.99	28.12	2.27
Pre-sintered	0.89	26.83	2.2
Sintered	0.86	24.67	–

The measurement was performed in a sealed compartment flushed with a (H_2 4 vol.% in N_2) gas mixture, saturated with water ($p(H_2O) = 0.031$ atm) with a flow of 50 mL/min at 25 °C. This gas mixture corresponds to a $p(O_2)$ of 9.69E-14 Pa at 827 °C (1100 K).[7] After reduction of the NiO to Ni the impedance of the samples was recorded in the range of 0.5 Hz to 3 MHz at temperatures from 250 °C to 900 °C with a frequency response analyser (Solatron 1260). The recorded impedance spectra were analyzed with ZView 2.80 (Scribner Associates, Inc.) software.

3. Results and discussion

Pressed and (pre-) sintered anode substrates showed good reproducibility and little deviation in weight, height and diameter after sintering. The substrates were all measured and weighed before and after (pre-) sintering, the mean values are summarized in Table 3.

The two YSZ powders from Unitec and Tosoh and the binders had an impact on the printability of the slurries as shown in Table 4. All pastes contained 2 mg m^{-2} dispersant calculated on the specific surface area of the YSZ powder.

After production the pastes were printed on plastic foils in order to check the printability. Good printability generally correlates with viscosities in the range from 4 Pa s to 12 Pa s at 100 s^{-1}.

An exception is paste B5, which was not suitable for printing despite of its viscosity around 10 Pa s, resulting from the dilatants behaviour at higher shear rates. Paste B0 did not yield a homogenous layer, most likely due to the low solid loading.

Table 4
YSZ electrolyte pastes

Powder	ID	η (Pa s) at 100/s	Binder wt.%	Powder vol.%	Applicability for screen printing	Binder system
FYT13-002H (Unitec)	A1	2	0	50	Possible	PVB Mowital B30H
	A2	4	0.1		Good	
	A3	6	0.25		Good	
	A4	14	0.5		Possible	
	A5	47	1		Not applicable	
TZ8-YS (Tosoh)	B0	7	0.25	20	Possible	
	B[a]	5	0.25	40	Good	
	B1	6	0	45	Good	
	B2	8	0.25		Good	
	B4[a]	20	0	50	Not applicable	
	B5	10	0.25		Not applicable	
FYT13-002H (Unitec)	C1	6	0.25	50	Good	PVB Mowital B20H
	C2	12	0.5		Good	
TZ8-YS (Tosoh)	D1	9	0.25	45	Good	
	D2	16	0.5		Possible	
Tosoh:Unitec (9:1)	M1	6	0.25		Good	

[a] Powder pre-treated at $T = 400$ °C.

The binder adjusted the viscosity to these needs and additionally stabilized the slurry against segregation. The pastes with the labels A3, A4, B0, B* and B2 containing the binder B30H and C1, C2, D1 and M1 with the binder B20H were applicable for screen printing and resulted in homogeneous layers. The pastes out of TZ8-YS powder achieved a maximum solid loading of 45 vol.%, while 50 vol.% of FYT13-powder was the maximum applicable powder concentration for the screen printing pastes.

The two dispersants Solsperse 3000 and polyvinylpyrrolidon (PVP) were compared on the basis of the recipe for paste B1. The rheological behaviour of the pastes without binder are displayed in Fig. 3.

The paste which contained Solsperse 3000 had the lower viscosity and showed a slight shear thinning behaviour, the pastes with PVP however had a strong dilatant behaviour at shear rates >10 s^{-1}. The chain length of the two polymers could be an explanation for the different behaviour: Solsperse 3000 possesses 66 C atoms, the vinyl chain of PVP between 40 and 600. The long chains of PVP might sterically interfere at higher shear rates, while at lower shear rates, the chains are more flexible and so the particles can float freely.

The influence of the binder content was studied for a constant solid loading of Unitec FYT13-002H powder. Fig. 4a shows that the viscosities are increasing with the binder content as a function of the shear rate, in Fig. 4b the viscosities at a shear rate of 100 s^{-1} were displayed as a function of the binder content.

The pastes A1-3 containing 0% to 0.25% of Mowital B30H have a sufficiently low-viscosity at high shear rates to be potentially suitable for screen printing. A1 however has a low-viscosity at low shear rates and is too liquid when filling the screen. The thixotropic behaviour of the pastes A2 and A3 with a binder content of 0.1 wt.% and 0.25 wt.% B30H classified these slurries as the most favourable for screen printing.

Pastes from the finer powder (Tosoh TZ8-YS) were expected to result in dense layers already at sintering temperatures lower than 1400 °C. Pastes containing a solid loading of 20 vol.%, 40 vol.%, 45 vol.% and 50 vol.% TZ8-YS powder and 0.25 wt.% binder B30H were compared (Fig. 5a). Heat treatment of the powder at 400 °C and 500 °C (Fig. 5b) was considered to improve the paste properties eliminating physisorbed and chemisorbed water.

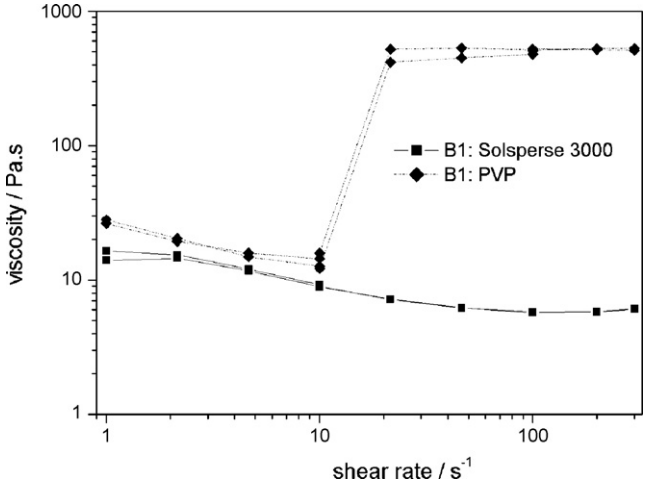

Fig. 3. Influence of the dispersants on the rheological properties of highly loaded (45 vol.%) zirconia dispersions.

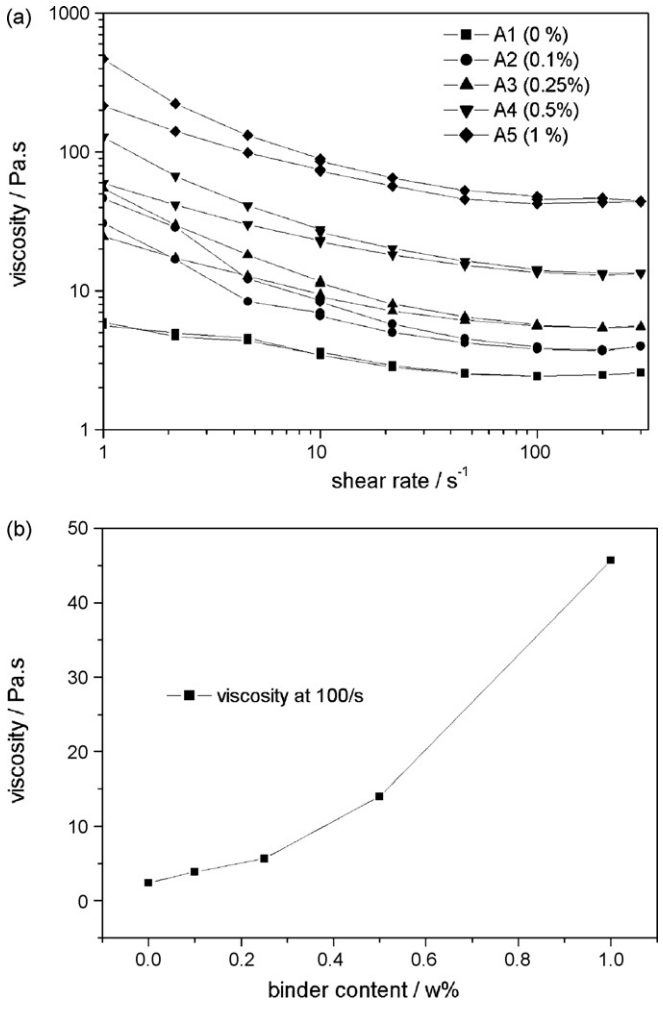

Fig. 4. Dynamic viscosity of pastes containing 50 vol.% FYT13-002H as a function of binder content (B30H).

The maximum solid loading for pastes containing TZ8-YS that were applicable for screen printing was 45 vol.% because pastes containing 50% show a strong dilatant behaviour at shear rates >100 s^{-1}. The untreated TZ8-YS YSZ powder has a BET surface area of 6.02 m^2/g while the heat treated powders resulted in 5.65 m^2/g and 5.61 m^2/g with a mass loss of 0.2%. The mass loss could be neglected and the influence on the specific surface area of the powders was small. The negative effect on the rheological behaviour of the heat treatment may be attributed to aggregates formed during the heat treatment.

The binder B20H has a lower average molecular mass than B30H and therefore investigated as a second binder system. The dynamic viscosities of pastes with contents of 0.25% and 0.5% B20H containing 50 vol.% FYT13-002H (C) and 45 vol.% TZ8-YS (D) powder are displayed in Fig. 6.

Comparing the pastes with either B20H or B30H as a binder, two main differences are obvious. First, the pastes containing B20H show lower viscosities at comparable shear rates, and second, the pastes show a dilatant behaviour at shear rates >100 s^{-1}.

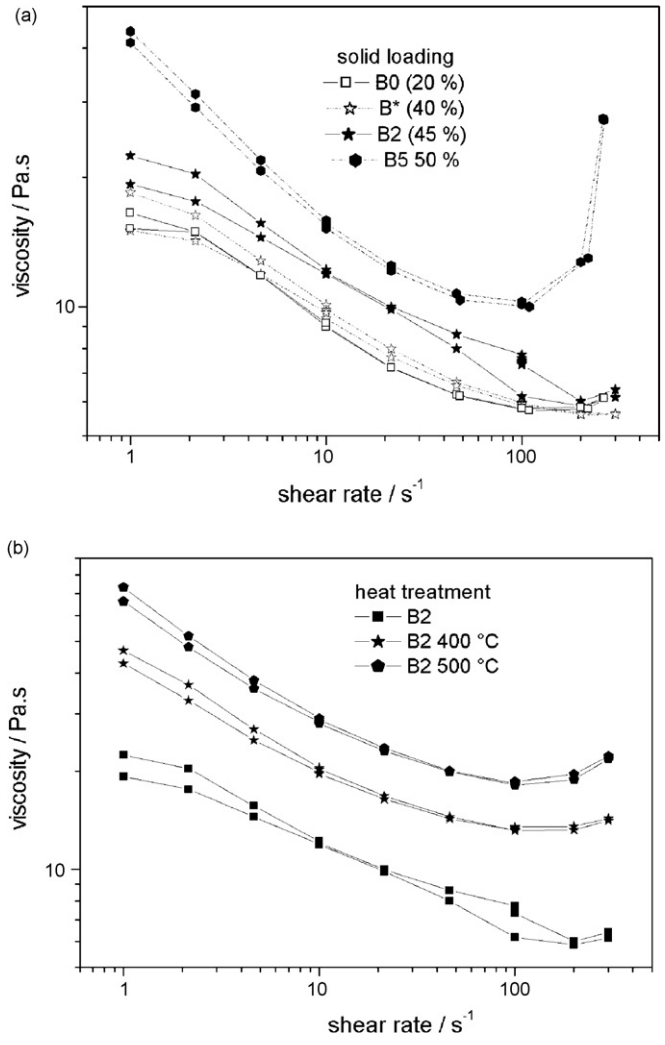

Fig. 5. (a) Influence of the solid loading of TZ8-YS powder on the dynamic viscosities. (b) Influence of the heat treatment of TZ8-YS powder on the dynamic viscosities.

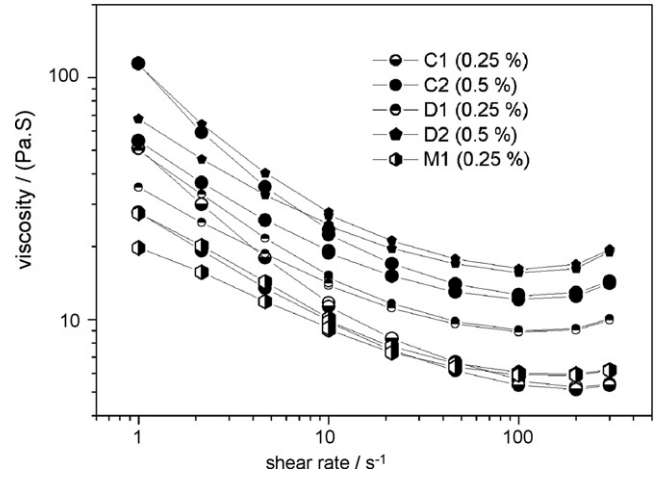

Fig. 6. Influence of B20H on the dynamic viscosities of pastes containing TZ8-YS and FYT13-002H YSZ powder.

The effect on the dilatant behaviour is even more pronounced at a binder content of 0.5% which may be attributed to the effect, that the formed network of B20H chains is more narrow and tighter compared to B30H. The preferred of the both tested binders to adjust the viscosity for screen printing was B30H. The viscosity of the pastes could be adjusted best with 0.25 wt.% of binder.

The coarser Unitec powder allowed a higher maximum solid loading (50 vol.%) than the finer Tosoh powder (45%) while still obtaining a printable paste.

The mismatch of the shrinkage between the anode substrate and the electrolyte layer was an important aspect when sintering the samples, which caused a bending of the towards the electrolyte side. Pastes with high solid loadings (45 vol.% and 50 vol.%) of YSZ powder resulted in less bending and cracks in the electrolyte layer than pastes with a low solid loading (20 vol.%). Bending could be also reduced by the pre-sintering of the anode substrates and the use of finer powder for the production of the anode substrates. Another study[8] demonstrated the influence of the pre-sintering temperature and the thickness of the anode substrate on the curvature of the samples as further aspects which can effect optimisation of the co-sintering.

Layers of paste B2, containing the Tosoh powder TZ8-YS were sintered at a temperature range from 1250 °C to 1430 °C and subsequently the microstructure was examined with a scanning electron microscope. The SEM micrographs Fig. 7a–d display the sintered YSZ layers with the interface to the Ni–YSZ cermet on the right side of the picture, where sample 7a and d correspond to one layer, b and c to two subsequently printed layers. The sample in Fig. 7a had a dwell time of 2 h at 1430 °C, while the samples displayed in Fig. 7b–d which were sintered at 1350 °C, 1300 °C and 1250 °C had a dwell time of 12 h.

It can be clearly seen that the number of pores in the electrolyte layer is increasing when the sintering temperature is reduced. The probability for the formation of interconnected pores through the electrolyte layer from 1430 °C to 1250 °C also increases due to this fact. However, to investigate the permeability of the layers, additional tests were necessary because SEM pictures do not give an answer whether the layers were gas tight or not.

In order to check the gas tightness visually crack free samples with two subsequently printed YSZ layers were tested by window leak test and He permeability test. The samples with sintering temperatures between 1250 °C and 1430 °C are listed in Table 5. Samples from Unitec powders are sintered at 1430 °C and labelled with "a", while samples from the finer Tosoh powder are sintered at lower temperatures. Furthermore the specific total resistance (R_{spec}) at 900 °C of the YSZ layer of dense samples and the activation energy (E_A) is displayed in Table 5.

The He-leak rate and the window leak rate for the last three samples are close to the criteria for practical fuel cell stacks (2E-5 hPa dm^3/s cm^2 for the He leakage test and 2.3E-4 hPa dm^3/s cm^2 for the window leak test[5]). The samples 73a, 80a and 102a therefore were considered to have dense electrolyte layers, while the samples 50 and 98 fail clearly by several orders of magnitude, indicating that a sintering temperature of 1430 °C is needed to obtain dense layers for the investigated slurries.

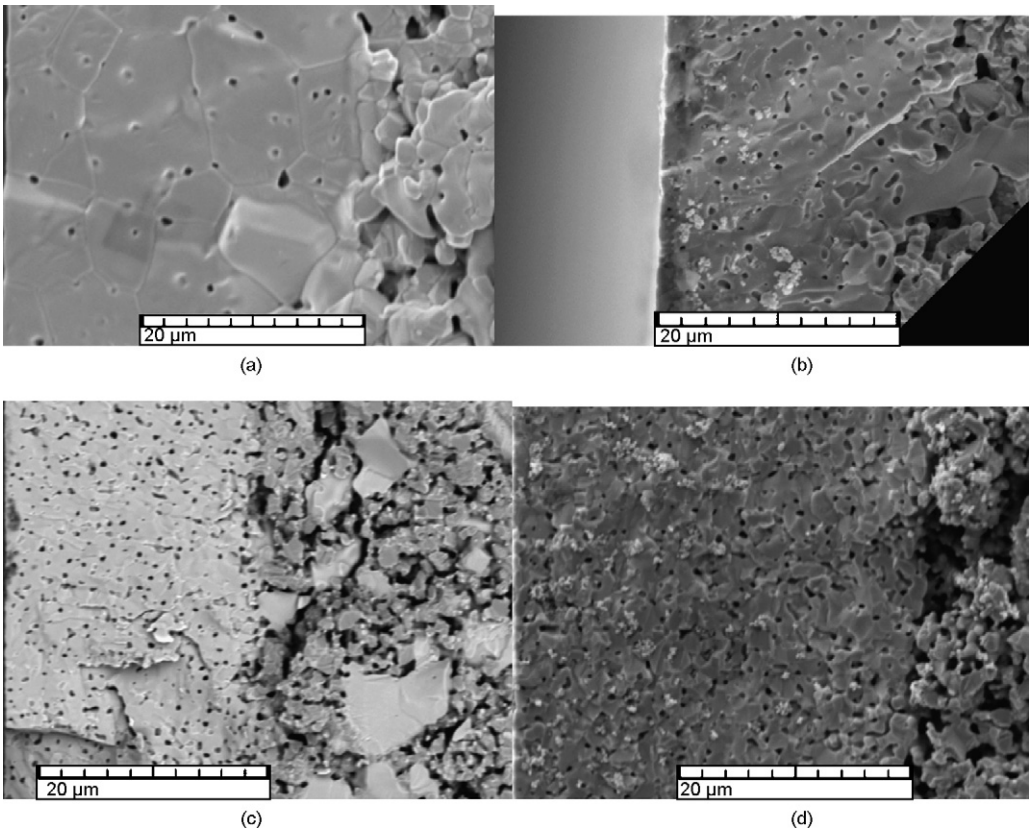

Fig. 7. SEM micrographs of layers out of pastes containing 45% TZ8-YS after sintering at 1430 °C (a), 1350 °C (b), 1300 °C (c) and 1250 °C (d) with electrolyte layer on the left and porous Ni–YSZ cermet on the right.

Impedance spectra of the samples 83a, 94a and 101a were recorded in a temperature range between 250 °C and 900 °C under reducing conditions in order to investigate the conductivity of the electrolyte layers. The Bode plots in Fig. 8a and b show the temperature shift in the impedance spectra of sample 101a, which is representative for all three samples. The spectra (Fig. 8b) recorded at temperatures between 256 °C and 477 °C show maxima between 10 kHz and 2 MHz, beginning with 366 °C to 895 °C, another maximum in the low frequency range is visible in the spectra. The maxima in the imaginary part (Fig. 8b) are attributed to different processes in the electrolyte, the YSZ/Ni anode and the Pt-electrodes. The Nyquist plots of two spectra (sample 101a) at 366 °C and 793 °C as well as the corresponding equivalent circuits of the fits are displayed in Fig. 9a and b.

The analysis of the electrode is complex due to the unsymmetrical arrangement of the electrodes (Fig. 2).

The impedance spectra in the temperature range from 256 °C to 477 °C were fitted with the equivalent circuits given in Fig. 9a and from 585 °C to 895 °C as in Fig. 9b with resistances (*R*), constant phase elements (CPE), an Open Warburg Element (Wo) and an inductance (L1).

The first semicircle at a temperature of 366 °C was fitted by a parallel arrangement of a resistor and a constant phase element (R1, CPE1) and (R2, CPE2) attributed to the electrolyte layer. Even though only one semicircle is observed, the unsymmetrical nature of the impedance response requires at least two RQ elements for the fit. Even though this model reflects the bulk and the grain boundary response, the correlation between the fit parameters is too high, in order to derive distinct values for each

Table 5
Gas permeability and total electric resistance of YSZ layers

Label	Sinter temperature (°C)	Dwell time (h)	Comments	He leak rates (hPa dm^3/s cm^2)	Window leak rates (hPa dm^3/s cm^2)	$\rho_{900\,°C}$ (Ω cm) (±2)	E_A (kJ mol^{-1}) (±2)
98	1300	12	Pre-sintered		0.9		
50	1350	12	Pre-sintered		2.4		
73a 83a	1430	2	No binder	7.1E-4 (73a)	1.3E-5 (73a)	27 (83a)	99 (83a)
80a 94a	1430	2	No binder	1.2E-5 (80a)	5.0E-5 (80a)	29 (94a)	97 (94a)
102a 101a	1430	2	Pre-sintered	3.5E-4 (102a)	6.0E-3 (102a)	30 (101a)	96 (101a)

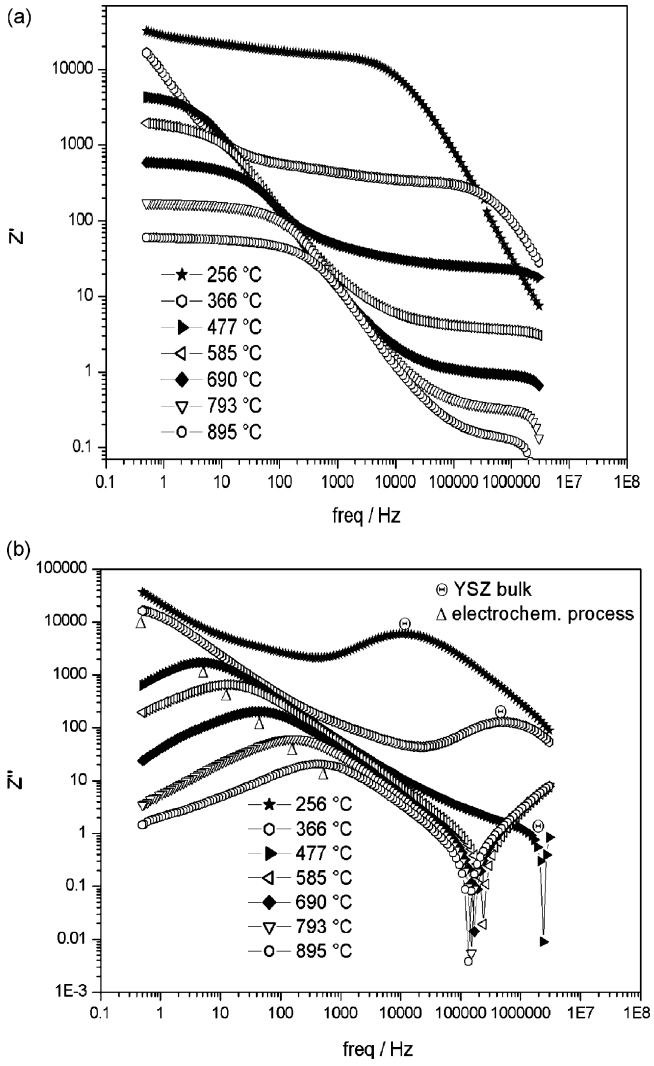

Fig. 8. Bode plots of sample 101a for various temperatures.

element in the fit. As a consequence only the sum of R1 and R2 can be derived representing the total electrolyte contribution to the impedance.

Furthermore, the assumption of diffusion in the anode described by Wo and R3 and CPE3 for the Pt electrodes were necessary to obtain a good fit for the electrode part. The inductance of the measuring wires is described by L1 at 796 °C, the intercept of the real axes (R1) represents the total resistance of the electrolyte, and the electrode processes can be described by R2, CPE2, R3 and CPE3.

The total electrolyte conductivity as a function of temperature is displayed in Fig. 10 and compares our results and with literature values[9–11] for dense YSZ. The activation energies were evaluated from the linear least square fits of the data points in an Arrhenius plot.

The three tested electrolyte layers show the same characteristics. The conductivity is lower than for a dense YSZ pellet, which was also measured and compared to literature values. This effect is also reported in literatures[8,12] for YSZ layers deposited by screen printing and centrifugal casting. The conductivity drop might come from the formation of a larger number of pores due to a lower sintering temperature.

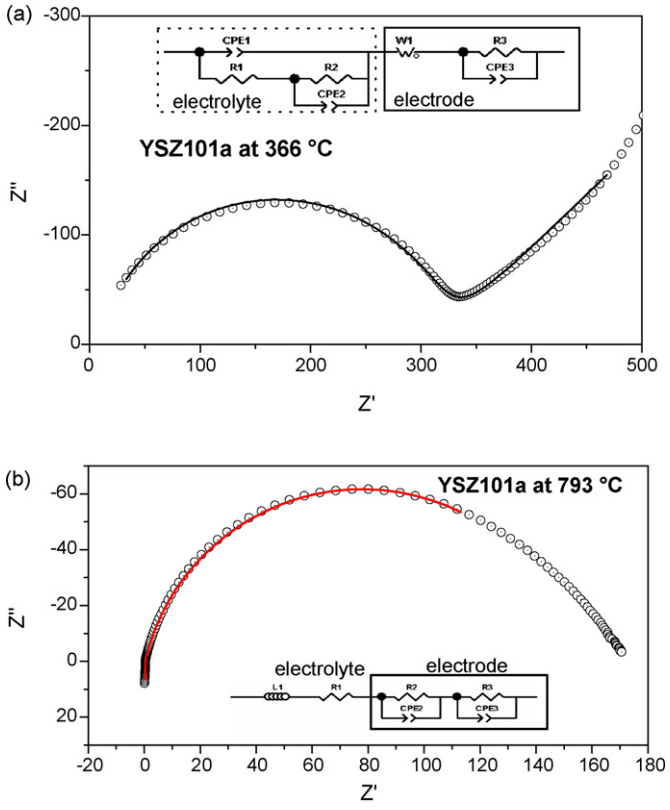

Fig. 9. (a) Nyquist plots of data at 366 °C with the corresponding fits (solid line). (b) Nyquist plots of data at 793 °C with the corresponding fits (solid line).

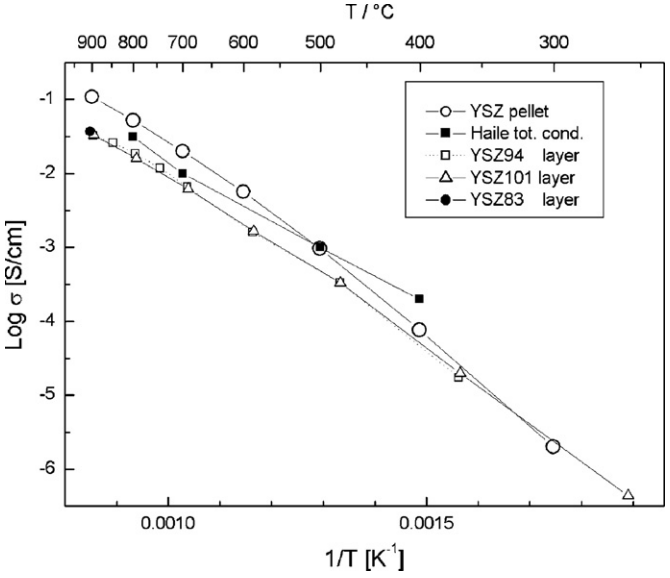

Fig. 10. Specific resistance at different temperatures in comparison with literature values.

4. Conclusions

Gas tight electrolyte layers for anode supported SOFCs have successfully been prepared by screen printing. Optimal print-

ing results were obtained using pastes with Mowital B30H as a binder and Tosoh and Unitec YSZ powders with solid loadings of 45% and 50%, respectively. Additionally, the pastes which resulted in gas tight layers showed thixotropic behaviour and viscosities $\leq$12 Pa s.

Sintering at 1430 °C leaded to dense and performing layers. The conductivities and activation energies are in agreement with the literature values, e.g. 46 Ω cm at 800 °C.[8] The sintering temperature could possibly be reduced further by the addition of nanosized powders or the use of a solvent containing dissolved ions of yttrium and zirconium for the preparation of the slurry.

Acknowledgements

The authors gratefully acknowledge the financial support from the EU-project "Real SOFC" (EC-Contract No.502612, SWISS contract SBF 03.170-2), technical support from Hans-Jürgen Schindler and Marie-Teres Gerhards and thank Wolfgang Preis for fruitful discussions.

References

1. Holtappels, P. and Stimming, U., Solid oxide fuel cells (SOFC). In *Handbook of fuel cells—fundamentals, technology and applications*, *1*, ed. W. Vielstich, A. Lamm and H. A. Gasteiger. John Wiley & Sons, Chichester, 2003, pp. 335–354.
2. Goldschmidt, A. and Streitberger, H.-J., *BASF—Handbuch Lackiertechnik, BASF Coatings AG*. Vincentz Verlag, Hannover, Münster, Germany, 2002.
3. Zuercher, S. and Graule, T., Influence of dispersant structure on the rheological properties of highly-concentrated zirconia dispersions. *J. Eur. Ceram. Soc.*, 2005, **25**(6), 863–873.
4. Kostogloudis, G. C., Tsiniarakis, G. and Ftikos, C., Chemical reactivity of perovskite oxide SOFC cathodes and yttria stabilized zirconia. *Solid State Ionics*, 2000, **135**, 529–535.
5. Menzler, N. H., Fleck, R., Mertens, J., Schichl, H. and Buchkremer HP, Application of wet chemical coating technologies for tubular SOFCs. In *Proceedings of the 5th European SOFC Forum, The European Fuel Cell Forum*, ed. J. Huijsmans, 2002, pp. 156–63.
6. Mücke, R. Sinterung von Zirkoniumdioxid-Elektrolyten im Mehrlagenverbund der oxidkeramischen Brennstoffzelle (SOFC). PhD Thesis, Ruhr-University, Bochum, 2007.
7. Lide, D.R. (ed.) *Handbook of Chemistry and Physics*. 83rd ed. CRC Press, Boca Raton, USA, 2002.
8. Dollen, P. and Barnett, S., A study of screen printed yttria-stabilized zirconia layers for solid oxide fuel cells. *J. Am. Ceram. Soc.*, 2005, **88**(12), 3361–3368.
9. Badwal, S. P. S., Zirconia-based solid electrolytes: microstructure, stability and ionic conductivity. *Solid State Ionics*, 1992, **52**(1–3), 23–32.
10. Park, J.-H. and Blumenthal, R. N., Electronic transport in 8 mole percent Y_2O_3–ZrO_2. *J. Electrochem. Soc.*, 1989, **136**(10), 2867–2876.
11. Haile, S. M., Fuel cell materials and components. *Acta Mater.*, 2003, **51**(19), 5981–6000.
12. Liu, J. and Barnett, S. A., Thin yttrium-stabilized zirconia electrolyte solid oxide fuel cells by centrifugal casting. *J. Am. Ceram. Soc.*, 2002, **85**(12), 3096–3098.